



SCIENCE OF TSUNAMI HAZARDS

Journal of Tsunami Society International

Volume 32

Number 3

2013

NUMERICAL MODEL STUDY OF TSUNAMI GENERATED BY POTENTIAL EARTHQUAKE WITHIN THE KOMANDORSKY SEISMIC GAP IN THE WESTERN ALEUTIAN ISLAND ARC

R. Kh. Mazova¹, B. V. Baranov², L. I. Lobkovsky², N. A. Baranova¹,
K. A. Dozorova², O. N. Chaykina²

¹Nizhny Novgorod State Technical Institute, Nizhny Novgorod, raissamazova@yandex.ru

²P.P. Shirshov Institute of Oceanology RAS, Moscow, bbaranov@rambler.ru

ABSTRACT

The Komandorsky seismic gap has distinctive boundaries and a length of 650 km. Its period of “seismic silence” comes close to the maximum recurrence interval for great earthquakes in the Aleutian Island Arc - the stress concentration here probably having reached the critical value. So, estimation of possible earthquake and tsunami characteristics within this gap becomes a significant problem. The closest analog of a similar gap is the area where the 2004 Sumatra-Andaman catastrophic event occurred. Thus, for the present study we used the same modeling scheme as we used for that event. It was assumed that a source length of 650 km, consisting of 9 blocks, and an earthquake with a moment magnitude $M_w=8.5$. Several block motion scenarios were considered. The tsunami generation and propagation in the Pacific Ocean and the possible wave characteristics on near and far-field coasts were estimated. Modeling of such an event showed that the wave heights on different Pacific coasts will vary from 3 to 9 meters. A tsunami wave with a 9-meter height is capable in causing significant loss of human life and economic damage.

Keywords: *Komandorsky seismic gap, seismic forecast, earthquake source, tsunami source, tsunami modeling*

1. INTRODUCTION

The last decade of the 20th Century was characterized by a gradual growth in the number of great earthquakes. In the subsequent decade the growth increased by 2.5 times (AMMON, 2010) - thus the problem of forecasting great earthquakes and modeling their associated tsunamis became of vital importance. As a rule, it is well known that great earthquakes with magnitude $M_w \geq 7.8$ along subduction zones generate tsunamis. Recent great events indicated that tsunamis caused by far greater losses of human life and destruction of property than the seismic ground surface oscillations (AMMON ET AL., 2005; LAY, KANAMORI, 2011). The threat of the tsunami hazard extends not only to coasts near the generating source but also to far-field locations.

Many aspects of earthquake and tsunami investigations are interlinked. Different approaches are being used by investigations, but common objective of all is to forecast such disasters and their potential impact. Research investigations include: a) identification of potential hazardous sources (seismic gaps); b) study of their structure and seismic regime; c) numerical simulation of the propagation of the generated tsunami, and d) estimates of tsunami run up heights at near and at distant coastal areas.

The present study uses the location, time and source structure of a potential great earthquake capable of generating a tsunami, based on a block model ("keyboard model") of earthquake generation along a zone of subduction (LOBKOVSKY ET AL., 1991). The methodology being used is as follows: The island arc wedge is cut into separate major segments by transverse faults penetrating down to the top of the under-thrusting plate. These fault blocks of the island-arc wedge (keyboards) represent minor elements of interaction between the under-thrusting and overhanging plates. A typical block size is about 100 km. However, in some cases the energy is released simultaneously along several neighboring blocks and thus, the length of resulting great earthquake's source area corresponds to the total length of all these blocks.

Earlier in 2006, on the basis of this model, a seismic forecast was proposed for the Central Kurile seismic gap and a simulation was undertaken of the generated tsunami by the predicted earthquake (LOBKOVSKY AT AL, 2006). On November 15, 2006 a great earthquake ($M_w=8.3$) occurred in the predicted area, which generated a significant tsunami (LAVEROV AT AL, 2007). Data obtained after this event demonstrated reasonably good correlation with the calculated values and thus confirmed the validity of the forecast and of the tsunami simulation (LOBKOVSKY ET AL, 2010).

In the present work, the same approach was applied to estimate the seismic potential of the Komandorsky seismic gap located in the Western Aleutian Island Arc, as well as for the numerical simulation of propagation and run-up of the tsunami that can be generated by such potential earthquake source.

2. THE KOMANDORSKY SEISMIC GAP

2.1. General Characteristics

Investigation of Aleutian Island Arc seismic activity has shown that great earthquakes within the arc occurred during separate time intervals. One seismic gap period in part of the arc lasted from 1938 to

1965 (SYKES, 1971; McCANN ET AL., 1979; SYKES ET AL., 1981). Sources of these great earthquakes filled the frontal part of the Aleutian Arc, with the exclusion of three areas (Fig.1). Specific seismic gaps were identified and named as the Komandorsky, Unalaska and Shumagin regions (SYKES, 1971; HOUSE ET AL., 1981; DAVIES ET AL., 1981). The term “seismic gap” is used for areas of seismic belts in island arcs and active continental margins, where great earthquakes did not occur during the last 50-100 years. Such gaps are regarded as the most possible earthquake sites for future events (FEDOTOV, 1965; McCANN ET AL., 1979; MOGI, 1968A; NISHENKO, 1991). After 1965, three great earthquakes with moment magnitude $M_w \geq 7.8$ occurred within the Aleutian Arc. However, their sources did not “fill” the seismic gaps listed above, thus these regions are still considered as the most hazardous parts of the arc (RUPPERT ET AL., 2007; WESSON ET AL., 2008; BARANOV, DOZOROVA, 2010).

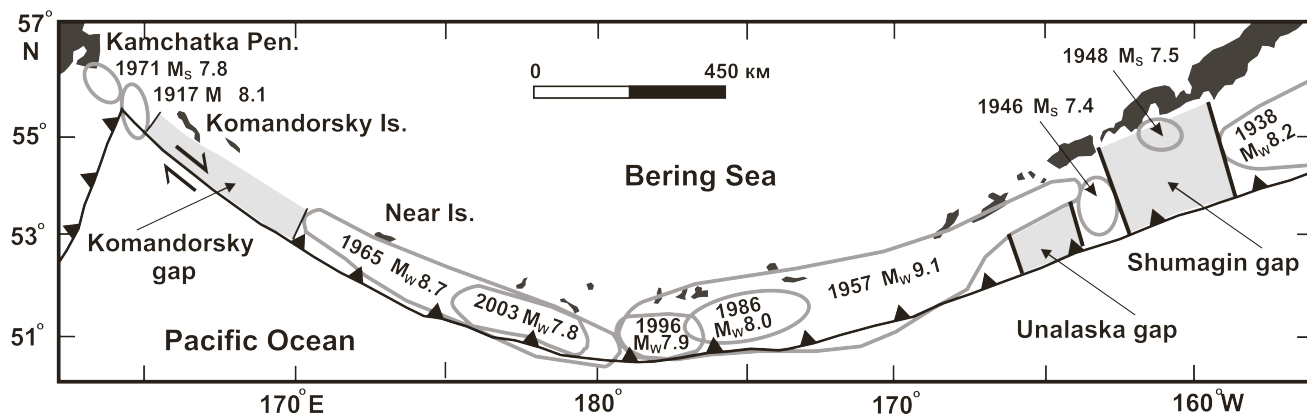


Figure 1. Location of earthquakes sources ($M \geq 7.4$) and seismic gaps in the Aleutian Island Arc after (Sykes et al., 1971), with addition of earthquake sources in 1986, 1996 and 2003. The Line with the triangles marks the subduction zone; the line with arrows marks a transform fault.

The Komandorsky gap is located in the frontal part of the Komandorsky group of the Western Aleutian Islands. According to the historic record, two earthquakes with magnitudes $M=7.5 \pm 0.7$ occurred in the western part of the Aleutian Arc in 1849 and 1858, but there is no information on their source location (SYKES ET AL., 1981). During the entire period of instrumental observations, only one earthquake with magnitude of $M_w=8.1$ was recorded on 30 January 1917. Macroseismic data of the 1917 earthquake (VIKULIN, 1986) indicates the source to have been located in the Komandorsky segment of the Aleutian Arc. This quake's source had dimensions of 180x90 km, was oriented obliquely to the arc's strike (see Fig.1) and occupied only the northwestern part of the Komandorsky seismic gap. The remaining gap lies between the areas impacted by the 1917 and 1965 earthquakes, and has a length of about 550 km (see Fig.1). The total length of the Komandorsky gap - together with sources of events in 1917 and 1971 - is about 650 km.

The long-term absence of great earthquakes within the western part of the arc, indicates absence of crustal displacements along the boundary between the Pacific Plate and the frontal part of the

Komandorsky segment - suggesting consequently, accumulation of stress and of elastic deformation approaching a critical level. This supposition is supported by specific distribution of strong earthquakes with magnitudes of $M \geq 6$ (BARANOV, DOZOROVA, 2010) and data from GPS observations (AVE'LALLEMENT, OLDOW, 2000; LEVIN ET AL., 2006).

2.2. Earthquakes Distribution and Crustal Displacements

The distribution of strong earthquakes having magnitudes $M \geq 6$ is shown in Fig. 2. Most of their epicenters are located mainly in the rear parts of the Komandorsky block. In the frontal part, strong earthquakes were recorded only near the junction of the Aleutian and Kurile-Kamchatka trenches. The frontal region between the sources of the 1917 and 1965 earthquakes has been seismically inactive in 40 year period for the earthquakes with $M \geq 6$. This fact may justify that displacements between the North American and the Pacific plates to the west of 170° E occur mainly along the rear boundary of the Komandorsky segment. A section of the arc located between the source areas of the 1917 and the 1965 earthquakes, moves together with the Pacific plate. It has long been known that the western segment of the Aleutian Arc is not a subduction zone, but a transform fault (CORMIER, 1975). Analysis of all available earthquake mechanism solutions (RUPPERT ET AL., 2008) has shown that shear displacements prevail to the west of 170° E.

Also, GPS data confirms that blocks of the Aleutian Island Arc move in a western direction with an increasing shear component the displacement rates range accordingly from 3.1, to 9.6 and 31.4 mm/year, for the eastern, the central and the western parts of the arc, respectively (AVE'LALLEMENT, OLDOW, 2000). The displacement rate becomes even greater in the westernmost termination of the Aleutian Arc (the Komandorsky block) where oblique subduction transforms into strike-slip. The GPS measurements have shown such a trend during several years, with Bering Island approaching Kamchatka at a rate of about 50 mm/year (LEVIN ET.AL, 2006). This value constitutes about 2/3 of the convergence rate (79 mm/year) between the Pacific and Eurasian (Okhotsk) plates near the junction of the Aleutian and Kurile-Kamchatka trenches, (DEMETS ET AL., 1994). In this connection it is supposed (SELIVERSTOV, 2009) that presently right-lateral displacement of the Pacific plate relatively Komandorsky Basin structures mainly occurs not along the faults located in the frontal part of Komandorsky Block, but along the fault in its rear part. So, both GPS data and earthquake distribution point on coupling of Komandorsky segment and Pacific Plate and, consequently, there is concentration of stress and deformations on this boundary. This conclusion agrees with belief that Komandorsky Block is a seismic gap. Long-time "silence" of this seismic gap may be possibly explained by the specific structure of this part of the island arc.

2.3. Block Structure of Aleutian Arc and Komandorsky Seismic Gap

The Aleutian Arc consists of adjacent blocks of Earth crust with length from tens to hundreds of kilometers (GEIST ET AL., 1988). The blocks are bordered by canyons and they are also governed by faults, and cut the frontal (southern) part of the arc, transversally to its general strike. The canyons also border sources of great earthquakes, as for example those in 1965 and 1957. The sources of these events border along the transversal fault confined to Amlya canyon. The source area of the 1965 earthquake, stretches in a western direction for a distance 650 km and is limited from the west by the canyon system of the Near Islands. The source consists of three blocks with lengths ranging from 100 to 180 km. To the east from Amlya the canyon source of the 1957 earthquake stretches for a distance 1200 km. Also, this source consists of three large blocks with lengths ranging from 100 to 450 km. The source of the 1957 earthquake is more homogeneous than that of the 1965 event. This may imply that segments in the first case move as a single body and thus the length of earthquake faults reaches 1200 km (NISHENKO, MCCANN, 1979).

For the main Aleutian subduction zone, estimates of changes in stress orientation were obtained by the method of earthquake source mechanism inversion for main subduction zone (LU, WYSS, 1996). As a result, boundaries, along which the change of stress orientation occurs, were distinguished. The boundaries coincide with terminations of great earthquakes sources and fault zones. Marine expeditions to the Western Aleutians (SELIVERSTOV, 1998; BARANOV ET AL., 1991; GAEDICKE ET AL., 2000) provided evidence of the existence of several active faults, parallel to this section of the island arc (Fig. 2). Right-lateral dislocations along the fault system lead to forming pul-apart basins, which are located both in the rear and the frontal parts of the arc. The biggest among them is the Steller Basin (Fig. 3), which is formed immediately on the Aleutian Trench axis where the biggest displacement rates between Pacific and North American plates are supposed. The Steller Basin has

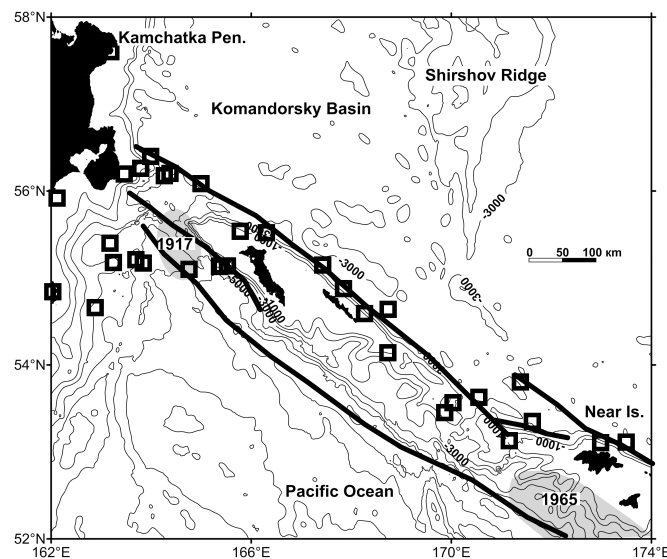


Figure 2. Distribution of shallow earthquakes in the Komandorsky segment from 1973 till 21.02.2013, $M \geq 6$, PDE Catalog. Thick lines mark dextral strike-slips, grey ovals indicate rupture zone of the great earthquakes. Contour interval is 1000 m, after (Smith, Sandwell, 1977).

typical rhomboid contours, which are governed by dextral shears of nearly NW strike and by normal faults of nearly NS orientation. To the southeast of the Steller Basin, numerous canyons cut the oceanic slope of the Komandorsky Islands to the point of Near Islands. The canyons correspond to the faults – they supposedly represent feathering structures of Komandorsky Shear Zone. Transversal faults cut the Komandorsky seismic gap into nine blocks with lengths ranging from 50 to 60 km (Fig.3).

Existing mathematical concepts at the present time provide the opportunity to create models of tsunami generation and propagation for different cases, including the simulation of tsunami from a source, consisting of several crustal blocks (LOBKOVSKY ET AL, 2006A; LOVKOVSKY ET AL., 2006B).

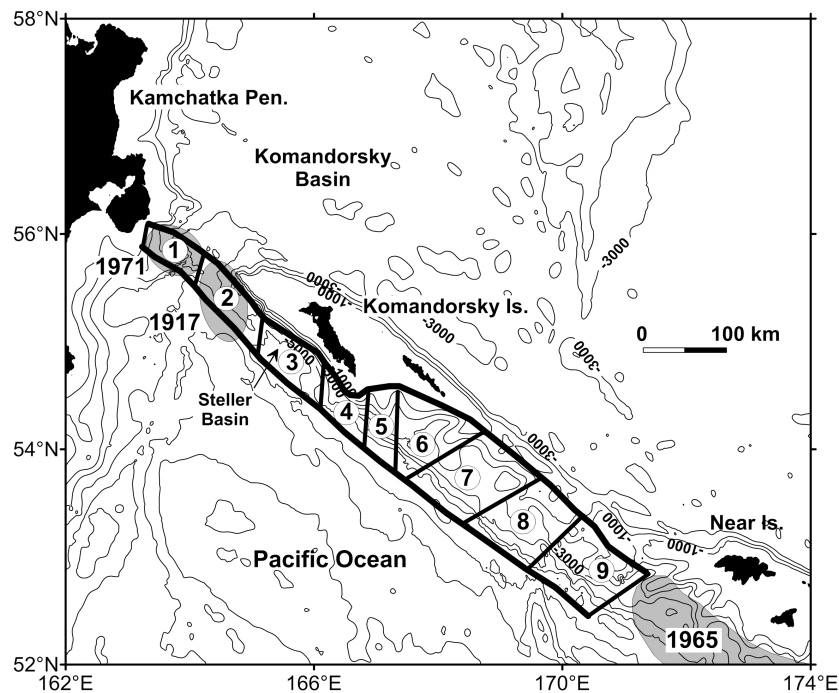


Figure 3. *Block structure of the Komandorsky seismic gap. Thick lines show dextral strike-slips, thin lines – scarps and canyons cutting the gap into 9 blocks. Grey ovals mark great earthquakes sources. Contour interval is 1000 m, after (SMITH, SANDWELL, 1977).*

2.4. The Problem Setting Boundary Conditions

The December 29, 2004, Sumatra-Andaman earthquake was used as an analog for the present simulation since it occurred under similar geodynamic conditions. Both, the Northern Sunda Arc and the Western Aleutian Arc are associated with zones of subduction, which subduction gradually change to dextral shear. Therefore, the scenario of a potential great earthquake along the Komandorsky gap area may be the same as that for the 2004 Sumatra-Andaman earthquake. The

latter event had a source area that was 1300 km in length and consisted of 9 to 12 sub-sources or blocks (AMMON ET AL., 2005; LAY ET AL., 2005). Fault rupturing occurred in a SE-NW direction during 10 minutes at the rate 2 km/sec (STEIN, OKAL, 2005). Peak displacements along the southern part reached 20 m (JI, 2005) and the tsunami source had a length 1000 km and a width of 250 km (FINE ET AL., 2005). In terms of the “keyboard model”, this event is interpreted as having nearly simultaneous dislocation of a large number of blocks-keys, triggering a giant earthquake source region that generated a mega-tsunami. As previously stated, a similar scenario is most probable for an earthquake along the Komandorsky seismic gap. Assuming that a future earthquake source will occupy the whole Komandorsky seismic gap, its source is estimated to be about 650 km its length, which would be half the size of the 2004 Sumatra-Andaman seismic source of the tsunami. Time parameters used for the simulation were based on this analogy. In the postulated model described by the present study, the fault rupture propagates in E-W direction and lasts 5 minutes (300 sec). The earthquake’s source region is cut into 9 blocks by transverse faults (Fig. 3). The displacements in the eastern segment of the fault are of the thrust type, while in the western segment are of strike-slip type. The magnitude of the potential earthquake is $M_w = 9.0$. The maximum height of block uplift in the eastern part is postulated to be 18m.

3. NUMERICAL SIMULATION OF TSUNAMI GENERATION AND PROPAGATION

3.1. Numerical model study

The following nonlinear shallow-water equations were used (Lobkovsky et al. 2006a) for the numerical simulation of the tsunami generated by a potential earthquake in the Komandorsky seismic gap.

$$\left\{ \begin{array}{l} \frac{\partial u}{\partial t} + u \frac{\partial u}{\partial x} + v \frac{\partial u}{\partial y} + g \frac{\partial \eta}{\partial x} = f_1 \\ \frac{\partial v}{\partial t} + u \frac{\partial v}{\partial x} + v \frac{\partial v}{\partial y} + g \frac{\partial \eta}{\partial y} = f_2 \\ \frac{\partial \eta}{\partial t} + \frac{\partial}{\partial x}[(\eta + H - B)u] + \frac{\partial}{\partial y}[(\eta + H - B)v] = \frac{\partial B}{\partial t} \end{array} \right. \quad (3.1)$$

where $f_1 = \frac{-C_h}{H + \eta} u \sqrt{u^2 + v^2}$, $f_2 = \frac{-C_h}{H + \eta} v \sqrt{u^2 + v^2}$ corresponds to the bottom friction;

x, y are the space coordinates along the axes Ox and Oy , respectively; t is the time;

$u(x, y, t), v(x, y, t)$ are the average over depth horizontal components of fluid flow rate;

$\eta(x, y, t)$ is the displacement of free surface relatively its undisturbed level;

H is the maximum depth of the basin at undisturbed water, function $B(x, y, t)$ describes displacement of bottom surface relatively to initial position (accounting dynamic characteristics of seismic motion);

g is the gravity factor, $C_h = \frac{(H + \eta - B)^{0.4}}{sh}$ is the bottom friction coefficient (Shezi coefficient), sh is the roughness coefficient.

A bathymetry map of the Pacific Ocean with resolution 1000m was used for modeling. A time step of 1 sec was chosen for the simulation and for each step, the wave failure conditions were checked. Specifically the modeling calculation area included a quadrant bordering from 125°E to 100°W and from 30°N to 60°N and the total network included $4042 \times 1808 = 7,307,936$ nodes. The total reflection condition (corresponding to a vertical wall boundary) was postulated in the last offshore point at a water depth of 10 m, which permitted fixing of maximum and minimum values of wave level displacement at this depth. There are many difference's schemes approximating Eqn. 3.1, but chosen for the present study was that of Marchuk et al. (1983), because it demonstrates high algorithmic flexibility. This scheme was used to take into account the kinematics and dynamics of motions in the earthquake source.

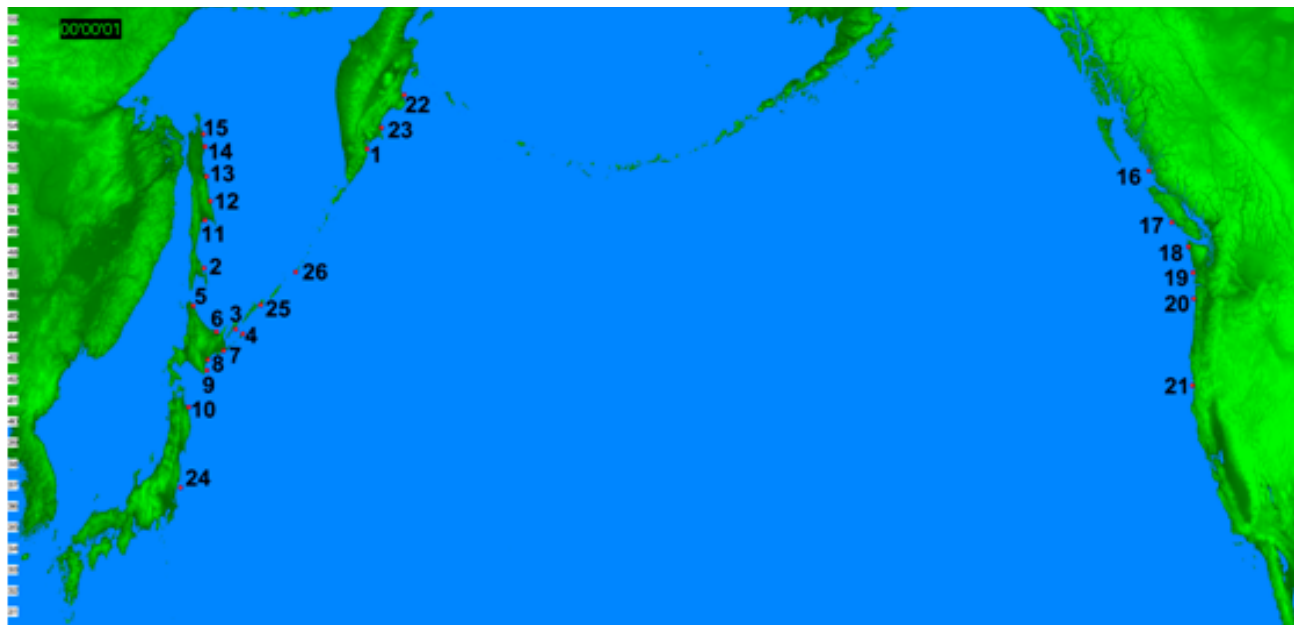


Figure 4. Segment of the Pacific Basin used for the numerical simulation. The locations of virtual tide gauges are marked by red dots and identified by numbers.

The calculations were carried out for the designated northern Pacific Basin segment and values were determined for the virtual tide gauges shown in Fig. 4. Data obtained from these tide gauges was used for the analysis of wave field characteristics in calculated water area.

Basing on the postulated type of realization of the potential earthquake process, computation of

tsunami source, generated by seismic source, was performed with the hypothesis that there is only vertical component in the displacement of the source blocks (see Fig. 4). Table 1 gives the top-plane coordinates of blocks, the beginning time of their uplift and the heights and time periods of such uplift. The tsunami source is formed during 300 seconds after the beginning of the earthquake and its source area develops from SE to NW direction. The tsunami source shape is directly affected by the given kinematics of the blocks in the earthquake source region (see Fig. 5 and Table 1). Finally, in using parameters of vertical displacement in the earthquake source for the simulation, it is also necessary to take into account the hydrodynamic character of the problem. In a case where the time of block uplifting is relatively small (see Table 1), instantaneous piston-type movement is realized. In such a case, due to water incompressibility and the hydrostatic character of pressure, the ocean

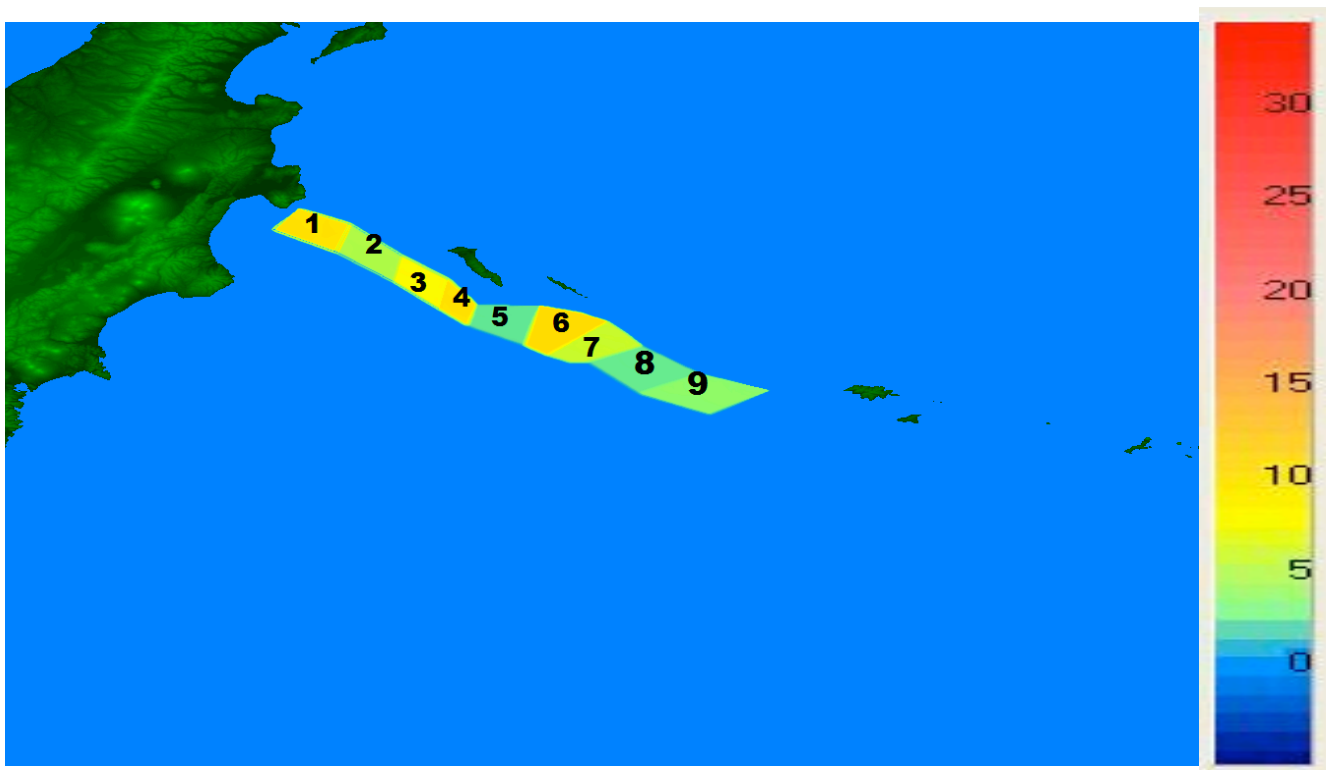


Figure 5. *Location of seismic source. The color of each block corresponds to its maximum vertical lift (the data are presented in Table 1), as well as to color scale presented on the right.*

water surface uplifts as much as the bottom block's surface (see Table 1). But in a case of slower uplifting of blocks 1-6, the wave height will decrease proportionally to $1/r^2$. So it becomes necessary to increase the initial displacement of the seismic source block in order to simulate correctly the water surface heights in the tsunami source (estimated by formulas which relate earthquake magnitude to resulting wave height). Thus vertical displacements in blocks 1-6 are assumed to be somewhat bigger than values calculated by these formulas. Forming such a source generates a tsunami and two processes occur simultaneously: wave generation by uplifting of next block in the seismic source and

the propagation of the wave from this block and wave generation from subsequent blocks. After the 6th minute, the generation process is terminated and only the process of wave propagation in the ocean is considered. Thus, chosen block kinematics in the seismic source region, lead to a complicated dynamic process affecting the whole ocean surface. In the present simulation the wave propagation was conducted for only a part of the Pacific Ocean, in directions, which included the Kurile Islands, the Okhotsk Sea and the central part of the western coasts of the North America.

Figure 6 represents characteristic time moments demonstrating the process of tsunami source generation. From this, and in accordance with chosen scenario (Table 1), it becomes obvious that the tsunami source region develops in SE-NW direction and that the source sharp depends directly on the postulated kinematics of the seismic source blocks.

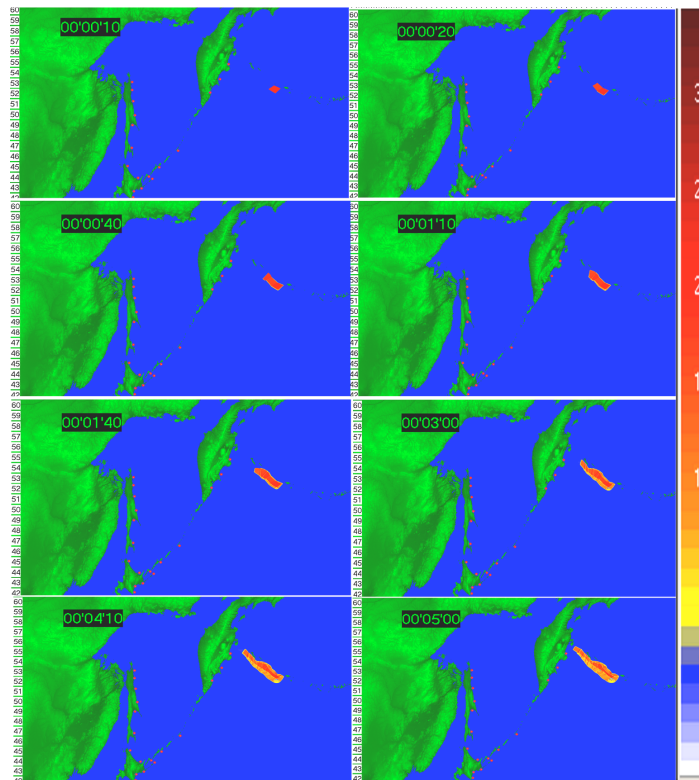


Figure 6. *Tsunami source generation by model seismic source.*

Table 1. Parameters of blocks (keys) movements for simulation

Block number	1	2	3	4	5	6	7	8	9
Block coordinates									
X1 (E)	164,37	164,37	165,37	166,17	166,67	167,67	168,07	168,77	169,67
Y1 (N)	54,53	54,53	54	53,53	53,235	52,883	52,706	52,588	52,034
X2 (E)	164,79	164,79	165,52	166,32	166,82	167,92	169,12	169,72	170,72
Y2 (N)	54,895	54,895	54,449	54,037	53,596	53,567	53,302	52,861	52,39
X3 (E)	163,4	165,37	166,17	166,67	167,67	168,07	168,77	169,67	170,89
Y3 (N)	54,845	54	53,53	53,235	52,883	52,706	52,588	52,034	51,671
X4 (E)	163,83	165,52	166,32	166,82	167,92	169,12	169,72	170,72	171,92
Y4 (N)	55,162	54,449	54,037	53,596	53,567	53,302	52,861	52,39	52,096
Start time, T_o , sec	250	180	130	100	70	40	20	10	0
Stop time, T , sec	300	250	180	130	100	70	40	20	10
Shift value, B , m	12	13	13	13	14	16	18	18	18

Data of 28 virtual tide gauges located along Pacific Ocean coasts (Fig. 1) were used for the analysis of wave field characteristics which were obtained as a result of the given scenario. The results of the calculation are presented in Table 2. Also indicated in this Table are the coordinates, the maximum and minimum wave heights at 10-meter isobath, the arrival phase of the first wave and the travel time for each point.

Figure 7 presents characteristic stages of tsunami wave propagation in the ocean for six characteristic moments: a) 2 h 13 min travel along Kurile islands; b) 2 h 45 min wave reaching Hokkaido Island; c) 3 h 53 min wave reaching the middle of Honshu Island; d) 4 h 43 min continuous tsunami propagation along Honshu Island and in the direction of western coast of North America; e) 6 h 23 min wave arriving at the coast of North America; f) 7 h 30 min wave continues propagation along the coast of North America.

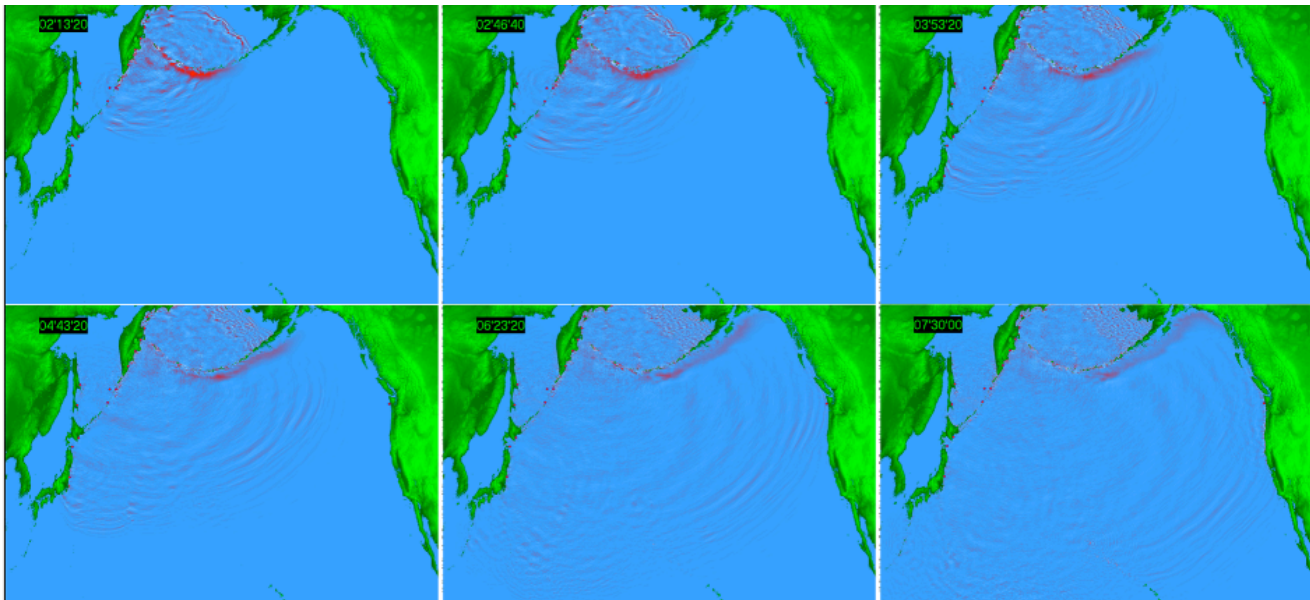


Figure 7. *Tsunami wave propagation in calculated basin at realization of given scenario for 6 time moments*

Analysis of the results obtained shows that the highest waves are observed along the east and southeast of Kamchatka (points 22 and 23) and on Simushir Island (point 26). Similarly, the results show that smaller amplitude waves penetrated through the Bussol and Krusenstern straits, further into the Okhotsk Sea and towards the eastern coasts of Sakhalin Island. The biggest among these waves are observed in points 2, 14 and 13. In points 2 and 14, the lowest run-down is recorded as well as the highest run-up (over 4.4 meters in point 14). Relative growth in tsunami wave height is observed near the Japanese Islands. Near Hokkaido Island (point 7) the tsunami is over 3 m high at the 10-meter isobath and near Honshu Island (point 10) the wave reaches a height over 2.5 m. It should be noted that at points 10 and 24 the intensive run-down is observed after first wave crest. Along the central parts of the western coast of North America, the highest tsunami wave heights are observed at points 19, 20 and 21, but also significant run-downs is observed as well.

Table 2. Results of the numerical simulation

Number of virtual tide gauge	Maximum wave height in point, m	Minimum wave height in point, m	Approaching phase of first wave	Approaching time of first wave
Sakhalin island				
2	3,06	-3,84	+	2 h 28 min
11	2,23	-2,70	+	2 h 31 min
12	2,98	-2,15	-	2 h 15 min

Number of virtual tide gauge	Maximum wave height in point, m	Minimum wave height in point, m	Approaching phase of first wave	Approaching time of first wave
Sakhalin island				
				min
13	2,52	-2,17	-	2 h 14 min
14	4,41	-3,85	-	2 h 23 min
15	1,49	-1,92	+	2 h 33 min
Kamchatka peninsula				
22	13,95	-10,94	+	18 min
23	10,27	-14,20	+	25 min
Kurile island arc				
3	2,34	-1,94	+	2 h 28 min
4	2,76	-2,65	+	2 h 21 min
25	3,31	-2,10	+	2 h 05 min
26	4,10	-1,12	+	1 h 27 min
Japan Honshu, Hokkaido				
6	4,13	-4,34	+	2 h 55 min
7	3,05	-2,24	+	2 h 45 min
9	1,43	-1,26	+	3 h 05 min

Number of virtual tide gauge	Maximum wave height in point, m	Minimum wave height in point, m	Approaching phase of first wave	Approaching time of first wave
Sakhalin island				
10	2,55	-1,78	-	3 h 31 min
24	3,95	-2,90	+	4 h 30 min
28	3,99	-3,69		4 h 13 min
Central part of western coast of the North America				
16	0,89	-1,26	-	5 h 45 min
18	3,22	-2,89	+	6 h 37 min
19	4,53	-3,64	-	6 h 48 min
20	3,79	-4,67	+	6 h 58 min
21	3,02	-2,96	+	7 h 50 min

Figure 8 demonstrates the distribution of maximum tsunami wave heights throughout the whole area of the investigation. The highest waves, designated by the yellow-colored areas, occur along the eastern

coasts of Kamchatka, the western and partly central Aleutian Islands, on the northeast coasts of the Kurile Islands and near small islands within the Bering Sea. Relatively high waves, designated by the red-colored areas are seen near Japan (Honsu and Hokkaido Islands), Eastern Sakhalin Island and the central part of North America's western coasts.

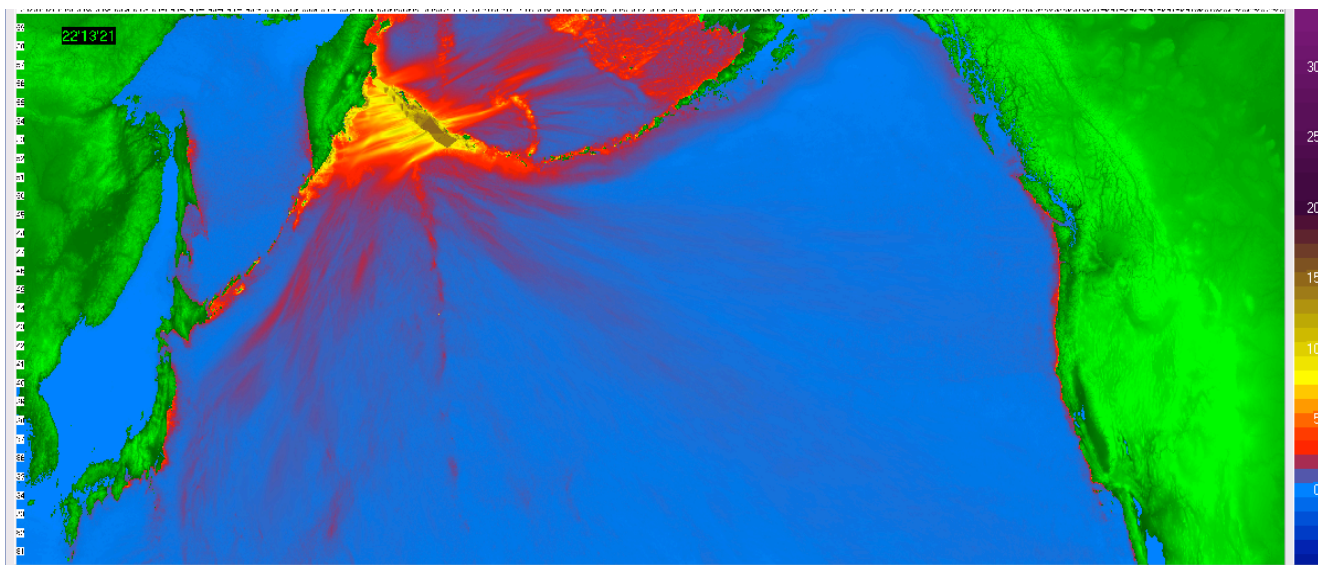
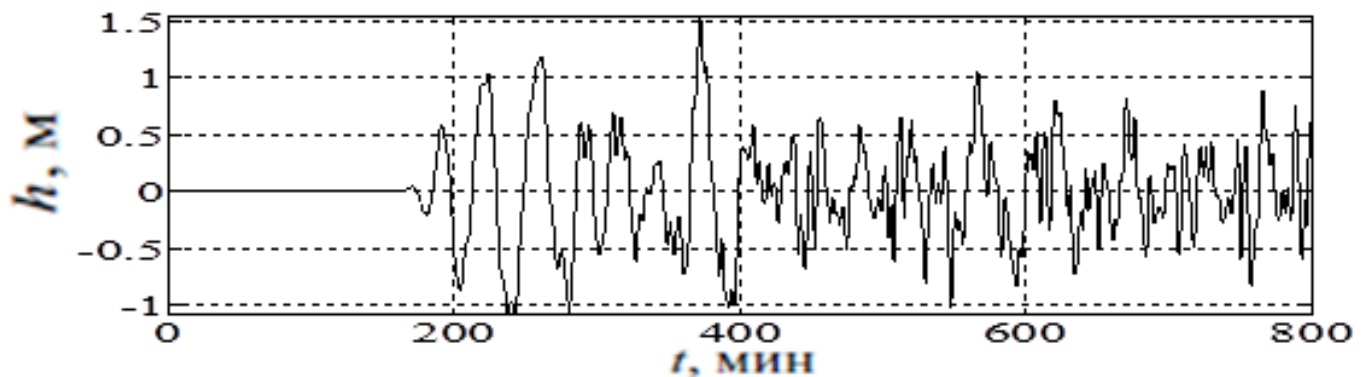


Figure 8. Maximum tsunami wave distribution in given basin as a result of numerical simulation
Vol. 32, No. 3, page 144 (2013)

3.2. Spectral analysis of wave characteristics

Based on the computation results obtained, a wavelet analysis was performed for points located near the Russian coast, the Japanese islands of Hokkaido and Honshu, as well as for points along the middle segment of the western coast of North America. Spectrograms constructed for points 12 and 14, located near Sakhalin Island, are practically close to those obtained by computations of wave fields from sources located in the seismic gap of the Middle Kuriles [Lobkovsky et al. 2010]. At the same time, spectral characteristics obtained by computation of wave fields from a seismic source located in the Aleutian seismic gap and for the region of Japan islands, have essential differences. Resonance effects arising between south Kamchatka and the western Aleutians where the seismic source is located can explain them. Long-term transitional processes (multiple re-reflections of waves) lead to the formation of numerous waves coming to Kurile Islands, as well as to the eastern coasts of Japan and to the central part of the western coast of North America. So, for point 26 located near Simushir Island (Fig. 9), there are well observed low-frequency intervals from 200 to 300 min and from 350 to 400 min. There are regions with frequencies equal to 1.5-2 cycles per hour (cph) that corresponds to a wave period 30-40 min, with intensity near 20 dB. In these time intervals all of the wave energy is concentrated in low-frequency interval. After 400 min all energy transfers to more high-frequency region excluding regions from 550 to 650 min.

For the same reason the part of high-frequency components is noticeably higher in tide gauge record for point 7. It should be noted that at such location of the seismic source, and hence, of the tsunami source, at all points where tide gauges are located, high-frequency components arise together with low-frequent or somewhat later. It depends on the character of wave interaction coming from the open sea and propagating along coasts and island chains. The latter give multiple high-frequency re-reflections.



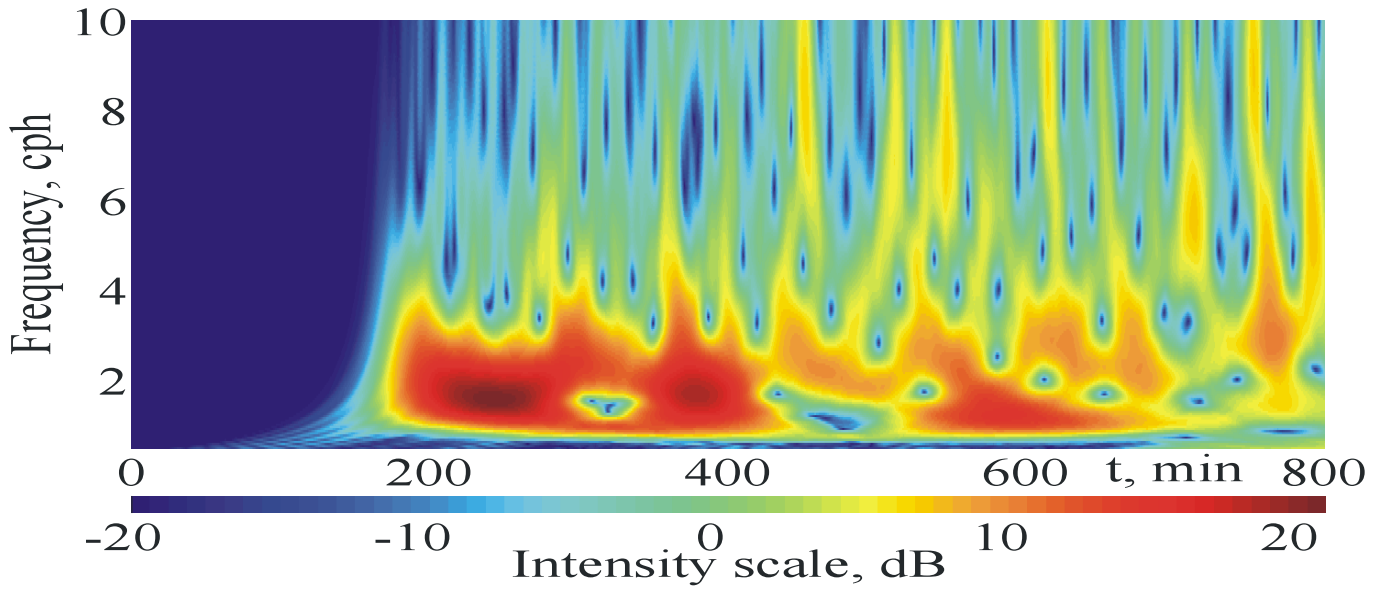


Figure 9. *The computed tide gauge records and spectrogram for point 26*

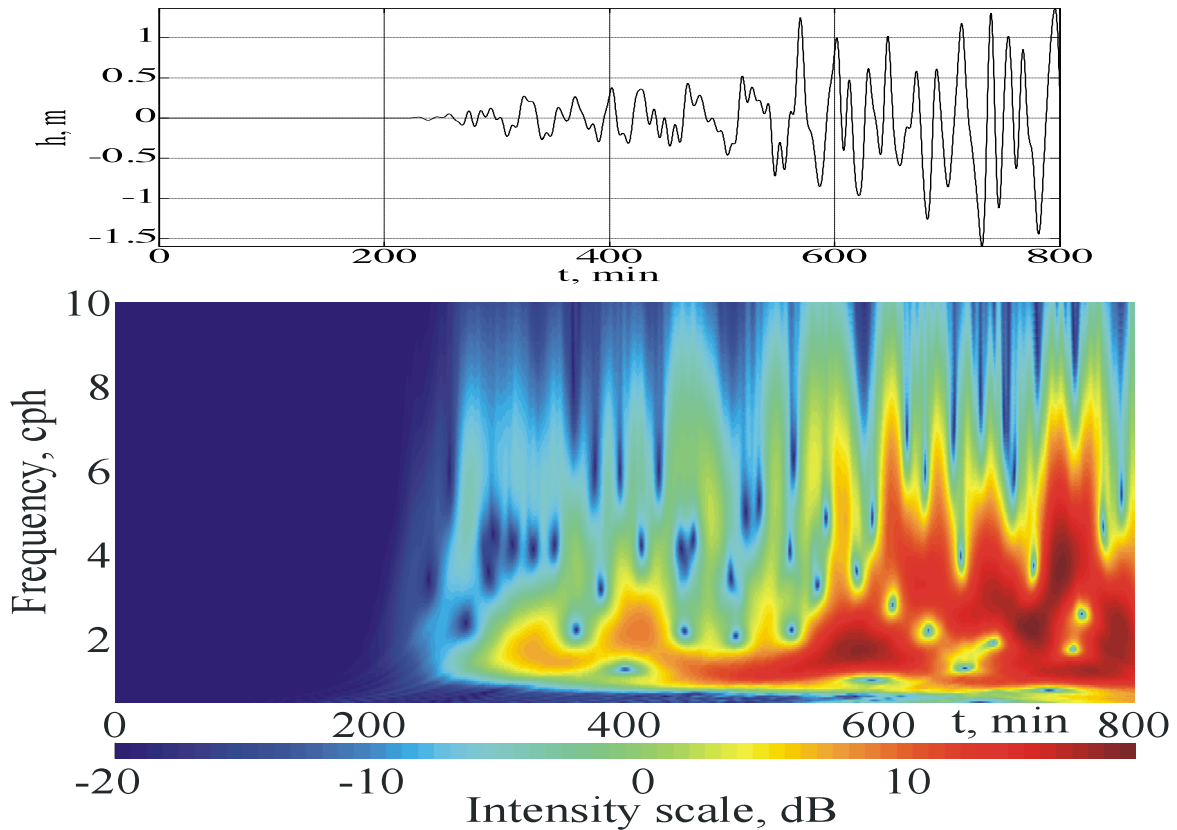


Figure 10. *The computed tide gauge records and spectrogram for point 7.*

At point 7, the low-frequency component is weak enough within the time interval ranging from 250 to 450 min. However, beginning from 450 min, the intensity of the low-frequency component increases and at 550-600 min range it reaches a maximum near frequency 2 cph, which corresponds to 30-min waves, with intensity near 15 dB. Approximately from 600 min to 750 min, most of the energy is concentrated in the range from 2 to 6 cph. One can distinctly see a low-frequency component in intervals 300-400 min, 500 min and further in the region of 700 and 750 min (with little gaps in intensity, but it is not essential against a background of intensive low-frequency regions). The low-frequency component is characterized by frequencies ranging from 1.5 to 2 cph and from 1.5 to 1 cph, which corresponds to 30-40 min and 40-60 min wave periods. The high-frequency components begin to manifest themselves at 450 min and are repeated regularly further after 30-40 min. One can see that the character of the spectrogram in the low-frequency region from approximately 250 to 400 min corresponds to the character of the spectrogram for point 26 in the range of 170-300 min. It is clearly seen that, in spite of the fact that point 7 is closer to point 26 as compared with point 9 (see Fig. 3), judging by the spectrogram character of the wave, the processes are more similar in points 9 and 26 than those in points 7 and 26.

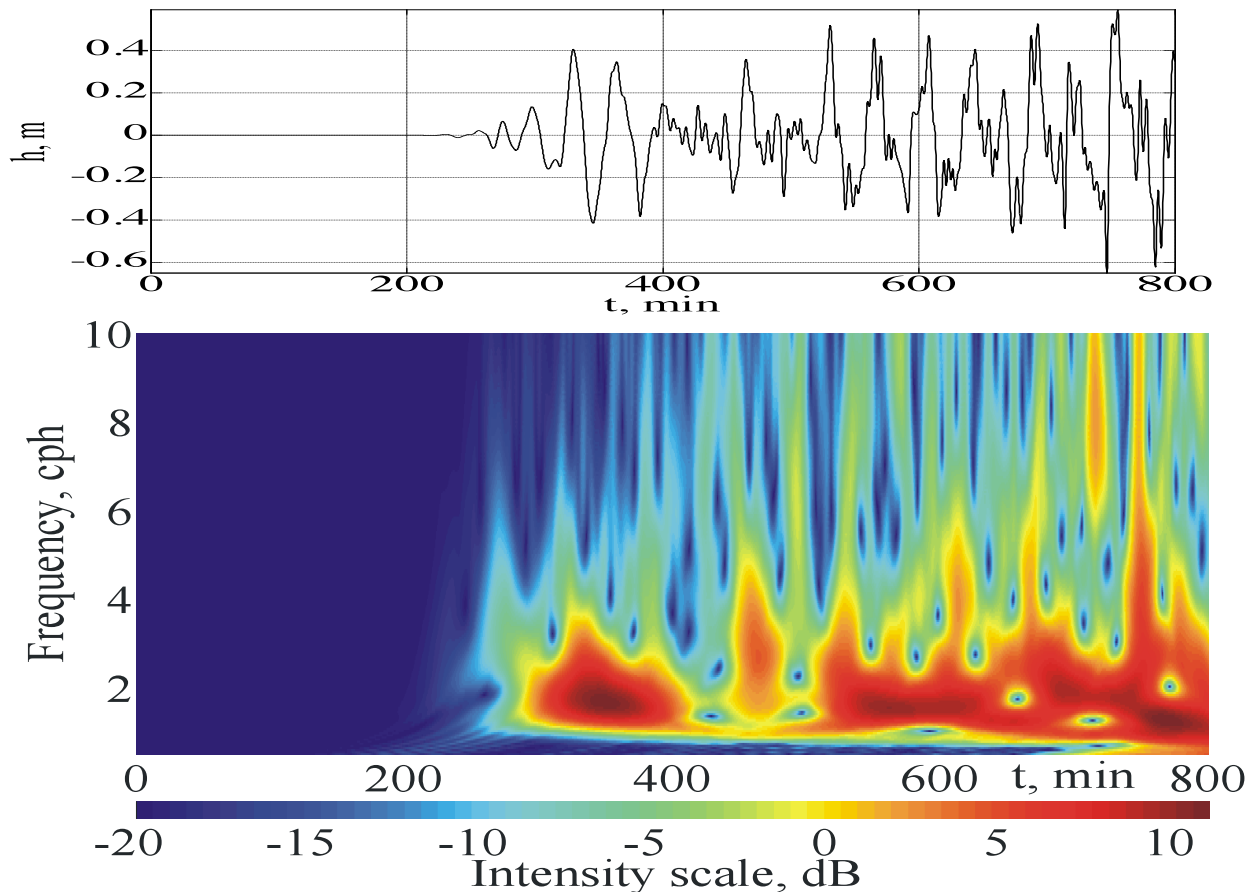


Figure 11. *The computed tide gauge records and spectrogram for points 9.*

Waves arrive at points 10 and 24 (Figs.12, 13) mainly from the open-sea direction, thus respectively, the portion of their high-frequency components in tide gauge records decreases. The component with frequency 2 cph (from 330 to 500 min, from 600 to 700 min) dominating at point 24 is significantly weaker as compared with that of point 10. At point 10, a low-frequency component prevails up to 450 min but its intensity is weak enough (about 7-10 dB). Regular, high frequency sparks of energy from 3 to 10 cph with intensity to 17 dB, appear after 450 min. At point 24, the low-frequency component occurs between the time-interval 330-500 min with little decay of intensity, which is again repeated during the time interval ranging from 600-800 min, for frequencies about 2 cph, i.e. 30 min waves. High-frequency components begin from 300 min and repeat up to 470 min. Afterwards, their intensity becomes weaker, though the regularity may still be traced. It should be noted that the initial frequency segment in many aspects repeats the character of spectrogram for point 26.

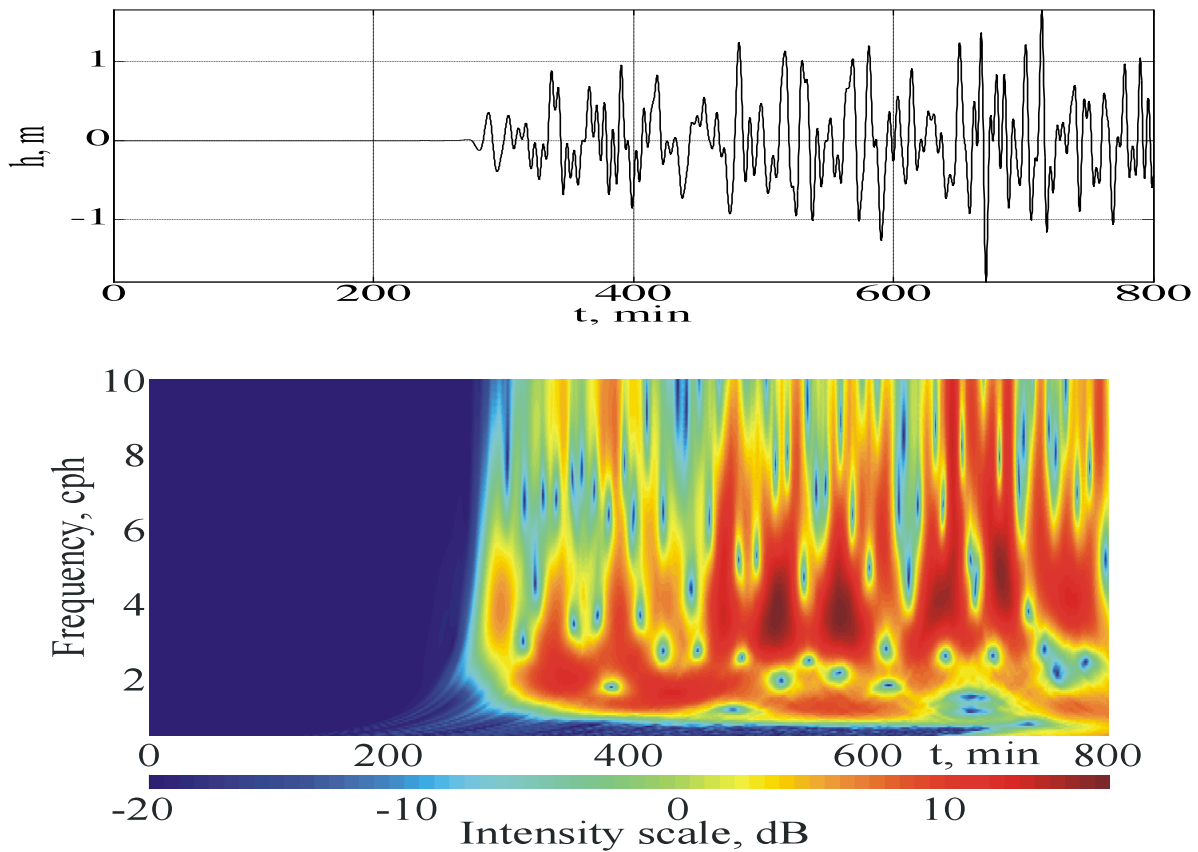


Figure 12. *The computed tide gauge records and spectrogram for points 10*

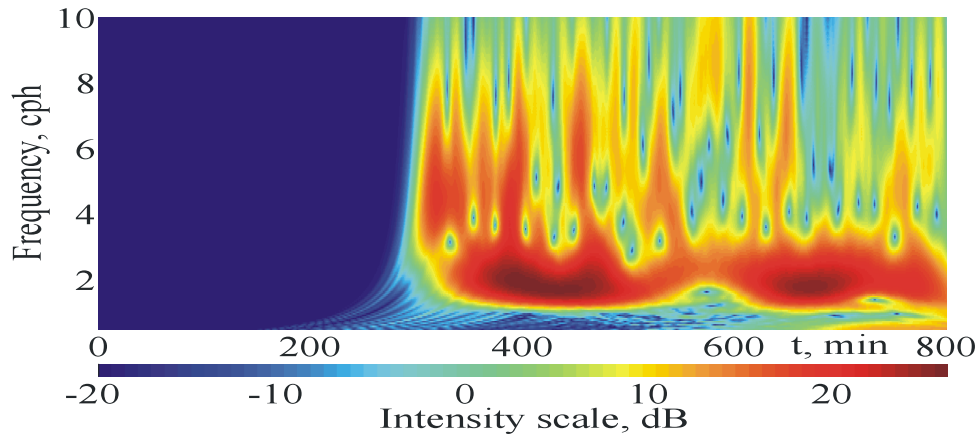


Figure 13. *The computed tide gauge records and spectrogram for points 24*

The waves come to points 19 and 17 (Figs. 14, 15) from an open-sea direction. The energy and wave frequency composition in points 17 and 19 are in many details similar. There is an increase of the wave's energy, with simultaneous broadening of the bandwidth occurs for these points beginning from 350 min. At point 17, beginning from 550 min, the energy increases. From 600 to 650 min a sharp spark appears and a local maximum is observed, approximately from 3 to 7 cph. The next local maximum is formed in the region of 750 min, from 1.5 to 5 cph (10-40-min waves). At point 19 in the range of 350-550 min, the intensity is low. From 550 to 750 min there is a sharp increase of intensity in interval from 1 to 6 cph (10-60 min waves). From 750 to 800 min, there is energy spark from 0.5 to 6.5 cph that corresponds to 2-hour waves with intensity 25 dB.

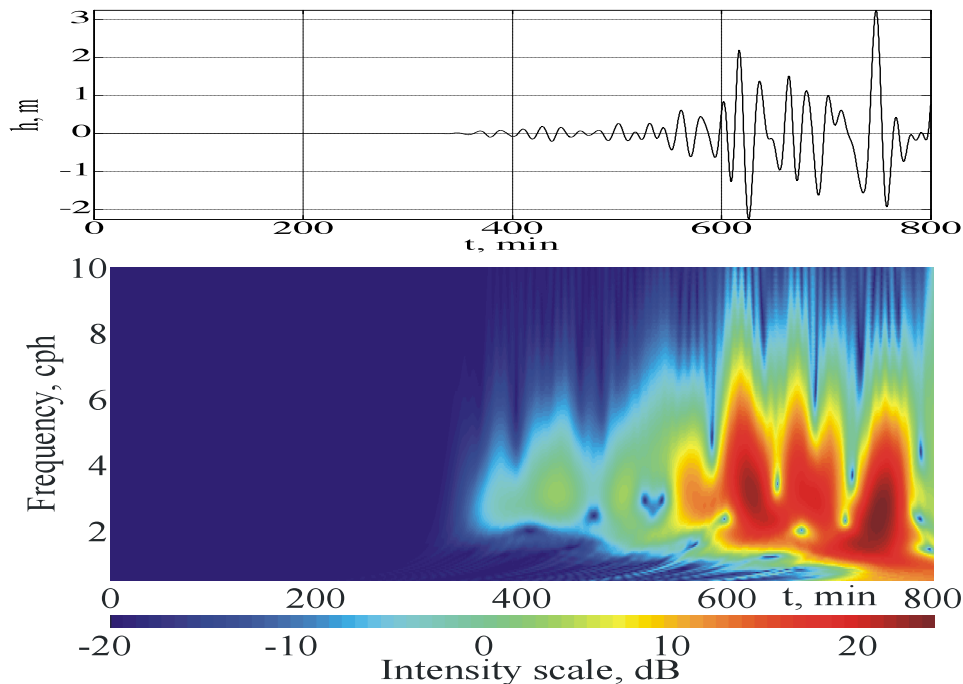


Figure 14. *The computed tide gauge records and spectrogram for points 17.*

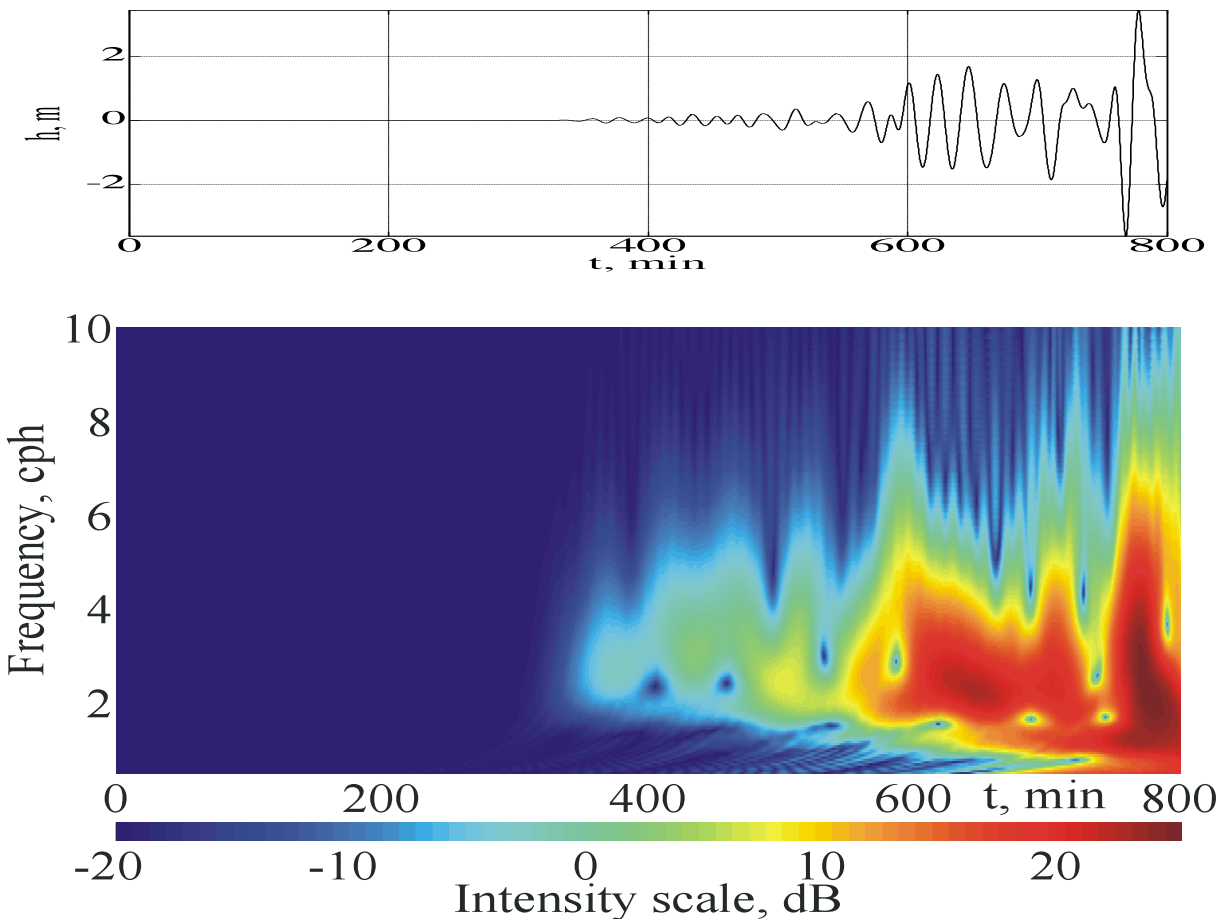


Figure 15. The computed tide gauge records and spectrogram for points 19.

4. DISCUSSION

As mentioned earlier, the main objectives of earthquake and tsunami source investigations are to forecast their occurrence and their environmental impact. Presently, there are three categories of seismic forecast: long-term, medium-term and short-term. The first two categories are considered below for the Komandorsky seismic gap.

A long-term forecast covering about 100 year time interval is based on investigations of seismic activity of most active subduction zones. The essence of the long-term forecast lies in distinguishing seismic gaps which are areas in regions of subduction zones in which areas great earthquakes did not occur for a long period of time (FEDOTOV, 1965; MCCANN ET AL., 1979; MOGI, 1968A; NISHENKO, 1991). The Komandorsky seismic gap was distinguished in the western part of Aleutian Island Arc in the framework of a long-term seismic forecast (SYKES, 1971). The recurrence interval for great earthquakes is unknown for this region - the last instrumentally recorded event with a reconstructed

magnitude of $M_w=8.1$ having occurred about 100 years ago in 1917. However, the source of this event included only the western part of the above-distinguished seismic gap. Analysis of historical documents shows that two earthquakes with magnitudes $M=7.5\pm 0.7$ occurred in the western part of the Aleutian arc in 1849 and in 1858, but it is impossible to determine the location of their sources (SYKES ET AL., 1981). Estimates of recurrence intervals for great earthquakes in the whole Aleutian Island Arc vary from 50 to 103 years (DAVIES ET AL., 1981). So up to now, a period of calmness has lasted for about 100 years - at least for the western part of the Komandorsky seismic gap - which corresponds to the maximum estimate of the recurrence interval for great earthquakes along the Aleutian Island Arc.

Instrumental observations and recordings of all great earthquakes on the Globe begun about 100 years ago. On the other hand, there are subduction zones areas - such as the Komandorsky seismic gap - where no great earthquake has registered during this period. Thus, an important question arises as to how the seismic potential of such an area may be estimated. This issue became extremely important after the December 26, 2004 Sumatra and the March 11, 2011 Japan disasters. Such catastrophic earthquakes and tsunamis forced many researchers to rethink that the seismic forecasts have been rather conservative. The forecasts were based only on data for the instrumental period of observations and did not take into account previous historical periods, when such catastrophes did occur but were not adequately documented.

Similarly, it was believed earlier that the Komandorsky seismic gap is unable to generate great earthquakes because of its specific structure (CORMIER, 1975). However, after the 2004 Sumatra-Andaman earthquake which occurred in a similar geodynamic situation, this belief has been revised and presently the seismic potential of the Komandorsky seismic gap is considered to be very high and may even generate an earthquake with a maximum magnitude of $M_{max}=9.2$ (Wesson et al., 2008).

The second category is the medium-term forecast. Its time interval covers from several days to several years. It is based on studies of ongoing processes immediately connected with preparation process of the fault, namely the transformation of stresses, the final stage of energy accumulation in seismogenic block and foreshocks (precursory shocks).

In many cases great earthquakes do not occur unexpectedly. As a rule, increases or decreases of seismic activity are observed shortly before a main quake strikes (WYSS, 1997). Foreshock activity appears several days, months or years before the main event for 10-30% of the total number of great earthquakes (SHIBAZAKI, MATSUURA, 1995; CONSOLE, MURRU, 1996; MAEDA, 1996). Such foreshock regularity has been observed for Aleutian Arc earthquakes. For instance, during the foreshock stage of the 1957 earthquake, seismic swarms occurred at both terminations of the source. At the western termination ($180^\circ W$) a seismic swarm appeared for three years before the main shock and in January 1957 a swarm was registered during one week at the eastern termination ($168^\circ W$) (HOUSE ET AL., 1981). Earlier, it was presumed that foreshock swarm in 1957 was caused by partial rupture which preceding the main faulting of this great earthquake. If a seismic gap had been previously distinguished for this area the appearance of these two distinct seismic swarms, could have served as a medium-term seismic forecast of the great earthquake of 1957 (HOUSE ET AL., 1981).

Seismic swarms, which may be interpreted as foreshock activity, had been also registered before the 2004 Sumatra-Andaman earthquake. On the southeastern boundary of its source, a series of a 17

earthquakes with one having a maximum magnitude 7.4 (PDE Catalogue) were recorded on November 2, 2002 - two years before the main 2004 event. The Sumatra-Andaman earthquake is considered here as being analogous of a possible, future, great earthquake in Komandorsky seismic gap. Thus, an increase of seismic activity around the gap and especially along its boundaries should be considered as a medium-term forecasting indicator – these facts have been pointed to preparation process of great earthquake in this area.

The numerical model study of tsunami generation and propagation from such a great earthquake in the Komandorsky seismic gap was performed on the basis of a numerical simulation, for the purpose of estimating the maximum wave heights that may be expected at a number of Pacific Ocean coasts. On Kamchatka, the tsunami waves can be expected to reach great heights throughout the whole coastline. Also, the Kurile Islands will undergo an intensive impact of tsunami waves propagating along their Pacific coasts, although the results of the present study indicate a decrease of energy in some parts of the island arc. In Sakhalin, the study indicates that the highest waves are observed in the northeast of the island. This can be easily explained by the influence of the most intensive wave front passing through the Krusenstern Strait and rotating obliquely to Sakhalin Island. On the Japanese Islands, significant wave heights can be expected - especially on the eastern coast of Hokkaido Island. The whole central part of the western coast of North America is expected to be impacted by tsunami waves originating from a great earthquake along the Komandorsky Islands region. Tsunami waves with heights ranging from 1.5 to 3 m at the 4 m isobate can demonstrate amplification in 1.5-3 times in the coastal zone (Pelinovsky, Mazova, 1992). Thus, the simulation shows that a potential great earthquake in the Komandorsky Islands can generate a tsunami that may cause real damage in many coastal areas of the Pacific Ocean and of the Okhotsk Sea.

The analysis performed by this investigation demonstrates that an extensive seismic source in the Komandorsky gap can generate a destructive tsunami, but that the character of the waves propagating in the Pacific Ocean essentially differs from those generated from a seismic source in the Central Kuriles. One of the principal aspects of this difference is in formation of kind of resonator under location of extended seismic source in the region of western Aleutes. The keyboard source, located in such manner, forms wave trains directed both along Kurile Islands chain and towards the open ocean. The effects of wave front interference are most distinctly manifested when the waves approach the Japan islands of Hokkaido and Honshu. This can be clearly seen in the constructed spectrograms of the data obtained from the selected virtual tide gauges along Japan's coasts. An analogous but less defined picture is observed for the spectrograms constructed with the data obtained from the selected virtual tide gauges along the central part of the western coast of North America.

5. CONCLUSIONS

Estimates of the recurrence interval for great earthquakes within the Aleutian Island Arc ($M_w \geq 7.8$) vary from 50 to 103 years, with the average recurrence being 80 years (Davies et al., 1981). The recurrence for great earthquakes in the Komandorsky seismic gap is estimated at 95 years - this being close to the maximum. This leads to the conclusion that seismic stress concentration has reached a critical value. The existence of such a gap in the western Aleutian Arc should be viewed as a long-

term forecast indicator, pointing to the high seismic potential of this area to generate a significant tsunamigenic earthquake.

As previously stated, the Komandorsky seismic gap has distinctive boundaries – in the east it was the source of the 1965 earthquake and in the west it was the source of the 1971 earthquake. Registration of strong earthquakes with magnitudes of $M \approx 7$ along the boundaries of the gap will be considered as medium-term forecast indicators pointing on to the potential, perhaps near-future occurrence of a great earthquake in this area.

Numerical simulation of a tsunami generated by the postulated source of this earthquake has shown that the wave heights on a number of Pacific coasts will vary from 3 to 9 meters. Tsunami waves with a 9-meter height are capable of far-field, inland inundation and destruction, which can cause significant human loss and economic damage.

ACKNOWLEDGEMENT

This work was supported by the Russian Foundation for Basic Research, project no. 12-05-00808.

REFERENCES

- BARANOV, B.V., DOZOROVA, K.A. (2010). Extension zones in Kurile-Kamchatka and Aleutian island arcs and long-term seismic forecast. *Physical, geological and biological investigations of seas and oceans*. Ed. R.I. Nigmatulin. Nauchnyi mir, Moscow, Russia. 280-300. (In Russian).
- VIKULIN A.V. (1986). Variant of long-term seismic forecast for Kamchatsky Bay and Kronotskiyi Peninsula. *Vulkanologiya i seismologiya* **3**,72-83. (In Russian).
- LAVEROV N.P., LOBKOVSKY L.I., BARANOV B.V., MAZOVA R.KH, KARP B.YA. (2007). Catastrophe on Sumatra: lessons and forecasts. *Nauka v Rossii* **1**, 4–11. (In Russian).
- LEVIN V.YE., MAGUS'KIN M.A., BAKHTIAROV V.F. AT AL. (2006). Multi-system geodesic monitoring of recent Earth crust motions on Kamchatka and Komandorskyskiye Islands. *Vulkanologiya i seismologiya* **3**,54-67.
- LOBKOVSKY L.I., MAZOVA R.KH., KATAEVA L.YU., BARANOV B.V. (2006). Generation and propagation of catastrophic tsunamis in the Okhotsk Sea water area. Possible scenarios. *Doklady Akademii Nauk* **410**,528-531. (In Russian).
- LOBKOVSKY L.I., MAZOVA R.KH., KISEL'MAN B.A., MOROZOVA A.O. (2010). Numerical modeling and spectral analysis of tsunami on November, 15, 2006 in Kurile-Kamchatka region. *Okeanologiya* **50:4**,1-10. (In Russian).
- SELIVERSTOV N.I. (1998). Structure of near-Kamchatka water areas and geodynamics of Kurile-Kamchatka and Aleutian island arcs junction area. Nauchnyi mir, Moscow, Russia. (In Russian).
- SELIVERSTOV N.I. (2009). Geodynamics of Kurile-Kamchatka and Aleutian island arcs junction area. KamGRU im. Vitusa Beringa. Petropavlovsk-Kamchatsky. Russia. (In Russian).
- FEDOTOV S.A. (1965). Regularities of distribution of strong earthquakes on Kamchatka, Kurile Islands and North-Eastern Japan. *Trudy IFZ* **36**, 66-93. (In Russian).

- AMMON C.J., C.JI, H.-K. THIO, ET AL. (2005). Rupture Process of the Great Sumatra-Andaman Earthquake. *Science* **308**,1133-1139.
- AVÉ LALLEMANT H.G., OLDOW J.S. (2000). Active displacement partitioning and arc-parallel extension of the Aleutian volcanic arc based on Global Positioning System geodesy and kinematic analysis. *Geology* **28:8**, 739-742.
- BARANOV, B.V., SELIVERSTOV, N.I., MURAVEV, A.V., ET AL. (1991). The Komandorskysky Basin as a product of spreading behind a transform plate boundary. *Tectonophysics* **199**,237-269.
- CONSOLE R., MURRU M. (1996). Probability gain due to foreshocks following quiescence tested by synthetic catalogs. *Seismological Society of America Bulletin* **86**,911-913.
- CORMIER, V.F. (1975). Tectonics near the junction of the Aleutian and Kuril-Kamchatka Arcs and a mechanism for Middle Tertiary magmatism in the Kamchatka Basin. *Geological Society of America Bulletin* **86**,443-453.
- DAVIES J.N., SYKES L., HOUSE L., JACOB K. (1981). Shumagin seismic gap, Alaska: History of great earthquakes, tectonic setting and evidence for high seismic potential. *Journal of Geophysical Research* **86**,3821-3855.
- DEMETS, C., GORDON, R.G., ARGUS, D.F., ET AL. (1994). Effect of recent revisions to the geomagnetic reversal time scale on estimates of current plate motion. *Geophysical Research Letters* **21**,2191-2194.
- FINE I.V., RABINOVICH A.B., THOMSON R.E. (2005). The dual source region for the 2004 Sumatra tsunami. *Geophysical Research Letters* **32**, L16602, doi:10.1029/2005GL023521.
- GAEDICKE, CH. BARANOV B., SELIVERSTOV N., ET AL. (2000). Structure of an active arc-continent collision area: the Aleutian–Kamchatka junction. *Tectonophysics* **325**,63–85.
- GEIST E.L., CHILDS J.R., SCHOLL D.W. (1988). The origin of summit basins of the Aleutian Ridge: implications for block rotation of an arc massif. *Tectonics* **7:2**,327-341.
- HOUSE L.S., SYKES L.R., DAVIES J.N., JACOB K.H. (1981). Identification of a possible seismic gap near Unalaska Island, Eastern Aleutians, Alaska. *Earthquake Prediction – An International Review Maurice Ewing Series* **4**, 81- 92.
- Ji C. (2005). Magnitude 9.0 earthquake off the west coast of northern Sumatra: Preliminary rupture model, report. U.S.Geol.Surv.,Denver,Colo.
http://neic.usgs.gov/neis/eq_depot/2004/eq_041226/neic_slav_ff.html
- MAEDA, K. (1996). The use of foreshocks in probabilistic prediction along the Japan and Kuril Trenches. *Seismological Society of America Bulletin* **86**,242-254.
- MCCANN, W., NISHENKO, S.P., SYKES, L.R., KRAUSE, J., (1979). Seismic gaps and plate boundaries: seismic potential for major boundaries. *Pure Applied Geophysics* **117**,1082–1147.
- MOGI, K. (1968A). Some features of recent seismic activity in and near Japan (1). *Bull. Earthq. Res. Inst. Tokyo University*. **46**,1225-1235.
- MOGI, K. (1968A). Development of aftershock areas of great earthquakes. *Bull. Earthq. Res. Inst. Tokyo University* **46**,175-203.
- LAY T., H.KANAMORI, C.J.AMMON, ET AL. (2005). The Great Sumatra-Andaman Earthquake of 26 December 2004. *Science* **30**,1127-1133.
- LAY T., KANAMORI H. (2011). Insight from the great 2011 Japan earthquake. *Physics Today* December,33–39.

- LOBKOVSKY L. I., KERCHMAN V. I., BARANOV B. V., PRISTAVAKINA E. I. (1991). Analysis of seismotectonic processes in subduction zones from the standpoint of a keyboard model of great earthquakes. *Tectonophysics* **199**, 211-236.
- LOBKOVSKY L. I., BARANOV B.V., DOZOROVA K.A., MAZOVA R. KH., BARANOVA N.A. The Komandorsky Seismic Gap: Earthquake Prediction and Tsunami Modeling // Proceedings of the Fifth International Tsunami Symposium (ISPRA-2012), Tsunami Society International, 3-5 Sept. 2012, Joint Research Centre, Ispra, Italy, 11page
- NISHENKO S.P. (1991). Circum-Pacific seismic potential, 1989-1999. *Pure and Applied Geophysics* **135:2/3**, 169-260.
- PELINOVSky, E.N., & MAZOVA R. KH., (1992), Exact analytical solution of nonlinear problem of tsunami wave runup on slopes with different profiles, *Natural Hazards*, **6(3)**, 227-249.
- RUPPERT N. A., LEES J. M., KOZYREVA N. P. (2007). Seismicity, Earthquakes and Structure Along the Alaska-Aleutian and Kamchatka-Kurile Subduction Zones: A Review. In: *Volcanism and Subduction: The Kamchatka Region Geophysical Monograph Series 172*. American Geophysical Union. 10.1029/172GM12, 129-144.
- SHIBAZAKI, B. & MATSU'URA, M. (1995). Foreshocks and pre-events associated with the nucleation of large earthquakes. *Geophysical Research Letters* **22**, 1305-1308.
- SMITH W. H. F., SANDWELL D. T. (1977). Global sea floor topography from satellite altimetry and ship depth sounding. *Science* **277**, 1956-1962.
- STEIN S., OKAL E. (2005). Speed and size of the Sumatra earthquake. *Nature* **434:7053**, 581-582.
- SYKES, L.R. (1971). Aftershock zones of great earthquakes, seismicity gaps, and earthquake prediction for Alaska and Aleutians. *Journal of Geophysical Research* **76**, 8021-8041.
- SYKES, L.R., KISSLINGER, J.B., HOUSE, L., DAVIS, J.N., JACOB, K.H., (1981). Rupture Zones and Repeat Times of Great Earthquakes Along the Alaska–Aleutian Arc, 1784–1980. In: Simpson, D.W., Richards, P.G. (Eds.), *Earthquake Prediction, an International Review*, Maurice Ewing Series, *AGU, Washington, D.C. Vol. 4*, 73–80.
- VOLTSINGER, N.E., KLEVANNY, K.A., PELINOVSky, E.N. 1989. Long-wave dynamics of coastal zone (Gidrometeoizdat, Leningrad, USSR, 1989).
- WESSON R. L., BOYD O. S., MUELLER C. S., AND FRANKEL A. D. (2008). Challenges in Making a Seismic Hazard Map for Alaska and the Aleutians. In: *Active Tectonics and Seismic Potential of Alaska Geophysical Monograph Series 179*. American Geophysical Union. P..10.1029/179GM22, 385-397
- WYSS M. (1997). Can earthquakes be predicted? *Science* **278; 5337**, 487-490.